Synthesis of Carbon Nanotube-Reinforced Al2024 Matrix Nanocomposite Using Flake Powder Metallurgy Method

F. RIKHTEGAR, S.G. SHABESTARI, and H. SAGHAFIAN

In current work, the flake powder metallurgy method was applied to achieve the uniform dispersion of carbon nanotubes (CNTs) within the Al2024 powder. For this purpose, the flake morphology of Al2024 powder with suitable diameter-to-thickness ratio (D/t = 85) was obtained after ball milling for 4 hours at 250 rpm and ball-to-powder ratio = 10. Then, the surface of matrix was modified by a hydrophilic polymer [polyvinyl alcohol (PVA)] to obtain the sufficient –OH group on its surface. Additionally, the refluxing of CNTs in nitric acid was performed at 393 K (120 °C) for 6 hours to functionalize the reinforcement by –COOH agent. After preparation of initial materials, the Al2024–1.5 wt pct CNTs suspension was stirred in a slurry at pH 3 until the color was changed in steady state from ink-like to transparent at pH 5. The hydrogen bonding was formed between the –OH groups of PVA coated Al2024 and –COOH groups of functionalized MWCNTs during the mixing step. Also, the temporary polarity could be considered between H^+ and $C_{12}H_{25}SO_4^-$ ions on the surface of constituents, which led to improvement in the CNT distribution due to the changing of suspension pH. Consequently, the homogenous dispersion of CNTs in Al2024 flaky powders resulted in a chemical reaction of constituents without any destructive effects of mechanical forces. The morphological changes of Al2024 powders were studied by scanning electron microscopy (SEM), and surface treatments were evaluated by Fourier transform infrared and Raman spectroscopies. The dispersion of nanocomposite powder was investigated through field emission SEM. Also, X-ray diffraction analysis was used to investigate the initial Al2024 powder and formed phases after the ball milling process.

DOI: 10.1007/s11661-016-3772-4
© The Minerals, Metals & Materials Society and ASM International 2016

I. INTRODUCTION

THE implementation of aluminum matrix nanocomposites reinforced by carbon nanotubes (CNTs) has been developed during last decades as a result of their good mechanical strength and lightweight properties.[1] Nevertheless, the agglomeration of CNTs within an Al matrix has remained a main challenge of nanocomposite synthesis. Consequently, the initial dispersion step can be introduced as a more important level of processing to achieve the homogeneous distribution of embedded CNTs in Al powder. Many different processing routes have been applied to reduce this critical problem in bulk nanocomposites manufacturing such as powder metallurgy (PM), casting, melt infiltration, metal forming, and the recent combinative techniques.[2–7] The PM methods have been found attractive for most researchers because of their lower temperature and the controllable interactions between the matrix and the reinforcement.[8–14]

The ball milling method has been used in many studies as a common route to produce Al/CNT nanocomposites. In this procedure, the mechanical forces are applied to break the CNT bundles and the mixing process is performed in a dry batch state.[15–22] The employed impact stresses can lead to destruction of the tube structure of CNTs, and finally, the expected mechanical strength cannot be accessible. The new solution ball milling route has been recently promoted to reduce the energy level of the process using an isopropyl alcohol based solution in containers of the planetary ball milling machine.[23]

In semi-wet procedures, the ultrasonic waves have been applied as a single step or combinative with low-energy ball milling to disperse the CNTs.[24,25] Also, the nanoscale dispersion method has been introduced as a novel semi-wet process that uses natural rubber to maintain dispersion of CNTs in metallic powder.[26–28] But the results show that the effectiveness of these techniques decreases in high content of CNTs in Al matrix.

The new category has been developed in PM processing during recent years, known as slurry based methods, which involve more complicated steps to produce Al/CNT nanocomposites. These methods apply the fluid

F. RIKHTEGAR, Postgraduate Student, is with the School of Metallurgy and Materials Engineering, Iran University of Science and Technology (IUST), 16846-13114, Narmak, Tehran, Iran. Contact e-mail: Foundryman84@gmail.com S.G. SHABESTARI, Professor, and H. SAGHAFIAN, Associate Professor, are with the Center of Excellence for High Strength Alloys Technology (CEHSAT), School of Metallurgy and Materials Engineering, Iran University of Science and Technology (IUST), 16846-13114, Narmak, Tehran, Iran.

Manuscript submitted April 10, 2016.
Article published online October 13, 2016

dispersive environment and chemical reactions to make the desired products such as flake PM (FPM) and in situ chemical vapor deposition (CVD).[29–31] In this group of PM processing, some important preparations are considered in raw materials before mixing of nanocomposite constituents.

The uniform dispersion of CNTs has not yet been observed in slurry-based routes because of the multiple variables of processing, especially for Al alloys matrices. Al2024 alloy is selected as a matrix for nanocomposite manufacturing process, whereas its initial powder is produced by mechanical alloying of pure elements or pre-alloyed powder resulting in gas atomization of ingots.[32,33] In most earlier research, the Al2024–CNT nanocomposite powder has been synthesized by a dry ball milling process and it is necessary to study producing Al2024–CNT powder using a slurry-based method such as FPM.

In the present research, the effects of morphological changes of Al2024 alloy powder, chemical modification of matrix surface with a hydrophilic agent, functionalization of CNTs with suitable refluxing process, and the role of interfacial chemical reactions between constituents were investigated in nanocomposite manufacturing by FPM procedure.

The novelties of this investigation are summarized to achieve the homogeneous dispersion of CNTs within Al2024 alloy with FPM method and to conserve the tube structure of CNTs without using any mechanical forces. Also, the FPM process was quantified with controlling ball milling variables [consisting time and ball-to-powder ratio (BPR)] to obtain fully flake-shaped Al2024 powder and pH of suspension during synthesis of Al2024–CNT nanocomposite.

II. EXPERIMENTAL

The initial multiwall CNTs were purchased through Sigma-Aldrich Corporation.*

*Sigma-Aldrich; American company with chemical and biochemical products.

The physical and structural characteristics of CNTs are shown in Table I.

This type of CNTs can be imagined as short fiber nanotubes with a medium aspect ratio. Also, Figure 1 shows the field emission scanning electron microscopy (FE-SEM) images of CNTs at two different magnifications.

The functionalization of CNTs was performed in concentrated nitric acid at 393 K (120 °C) for 6 hours to create the carboxyl (–COOH) agent on the external walls of CNTs. Afterward, the CNTs were entirely rinsed with distilled water to obtain pH 7 and dried in an oven at 393 K (120 °C).

The air-atomized Al2024 powders with particle sizes in the range of $45 < M < 100$ μm were used as starting material for the matrix. Figure 2 shows SEM images of initial Al2024 powder at two various magnifications. Also, the chemical composition of Al2024 matrix alloy measured by mass spectroscopy is demonstrated in Table II.

According to Table II, the elements of Cu and Mg are the main alloying elements in bulk Al. Other required materials for processing of Al2024–CNTs nanocomposite such as sodium dodecyl sulfate (SDS), stearic acid, and polyvinyl alcohol (PVA), with a molecular weight of 72,000 g/mol, were supplied through the Merck Group.**

**Merck Group; German company for high-tech products in healthcare, life science, and performance materials.

The FPM method was performed in five independent steps. Step 1 was defined to achieve the flake-like morphology of Al2024 powders, and it was evaluated by changing the variables of the ball milling process. The rotation speed of 250 rpm at different ball milling times of 2, 3, and 4 hours with a BPR ratio of 10 and 20 were examined for Al2024 alloy powder. The free volume fraction of 2/3 was used for each ball milling container.

In step 2, the aqueous solution was prepared by adding 2.0-mg/mL MWCNT-COOH and 1.5 wt pct SDS surfactant into deionized water. Continuously, the solution was placed in ultrasonic bath for 2 hours to get an ink-like dispersion.

Step 3 of the FPM method was followed to make the chemical modification of Al2024 flake powders with a PVA agent. Actually, this agent was used to establish the hydrophilic trait by –OH saturation on the surface of matrix powder.

For this purpose, the flaky Al2024 powder (10 g) was added to 3 wt pct PVA aqueous solution and it was magnetically stirred for 2 hours. Then, the PVA-coated powders were filtered and rinsed with deionized water and finally dried in an oven at 393 K (120 °C) with an argon-controlled atmosphere.

In step 4, the suspension was made from Al2024-PVA coated powder in water (100 mL) and then the pH of suspension was decreased to pH 3 by adding diluted nitric acid. The CNT aqueous solution was added drop-wise into Al2024-PVA suspension, and it was mechanically stirred until its color varied from dark into transparent at pH 5. The rotary evaporator was used at 333 K (60 °C) and a vacuum pressure of 75 mbar for drying of composite powder.

Table I. Physical and Structural Characteristics of Initial Carbon Nanotubes

Processing Method	Purity (Pct)	Aspect Ratio (L/D)	OD (nm)	ID (nm)	Length (μm)	Density (g/cm^3)	Type/Property
CCVD	90<	50 to 200	10 to 20	2 to 6	0.1 to 2	2.1	CNT

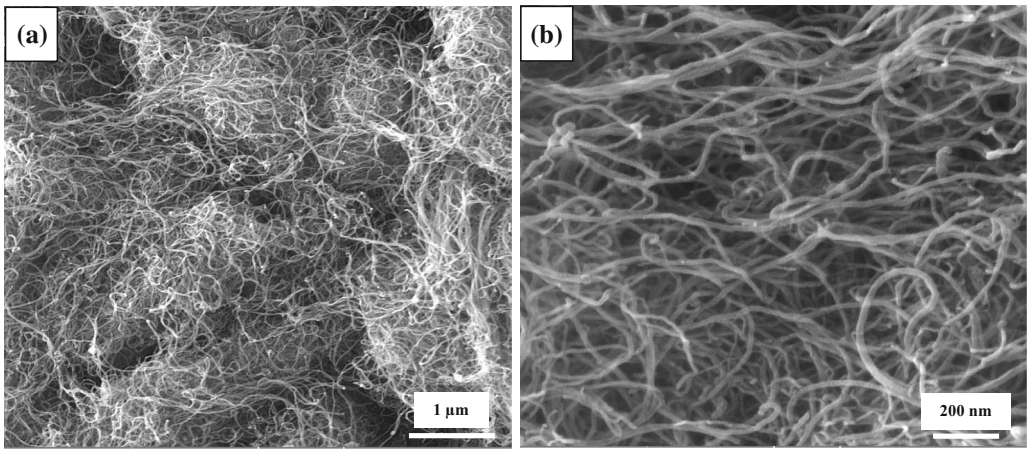

Fig. 1—FE-SEM images of initial carbon nanotubes at two different magnifications.

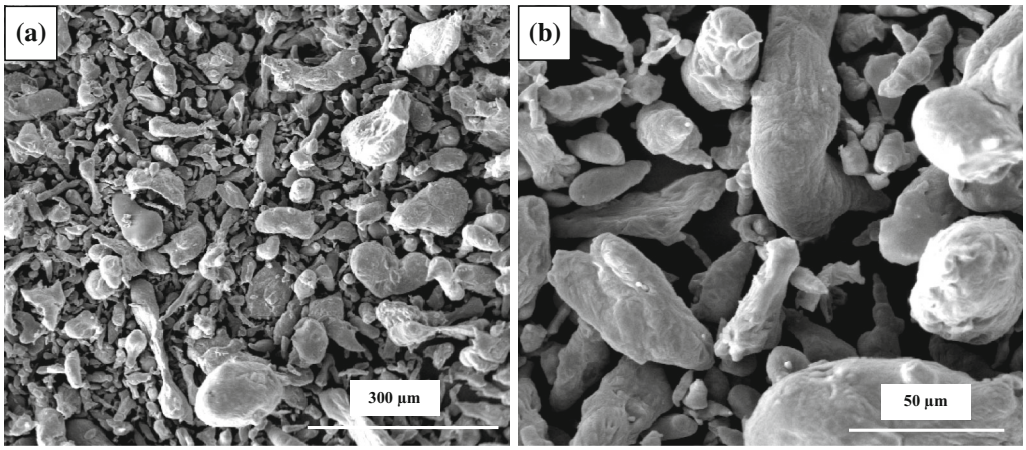

Fig. 2—SEM images of initial Al2024 powder at two different magnifications.

Table II. Chemical Composition of Al2024 Alloy

Al	Mn	Fe	Si	Mg	Cu	Elements
Bulk	0.35	0.27	0.83	1.75	3.23	wt pct

Step 5 was included in the calcination of Al2024–CNTs powders with flowing argon atmosphere at 773 K (500 °C) for 2 hours to eliminate the PVA coating from the composite powder. The volume fraction of CNTs within the matrix was considered in constant value (Al2024–1.5 wt pct CNT) in the FPM procedure.

The morphology of initial materials and dispersion of final products during the processing of Al2024–CNTs nanocomposite were studied using SEM and FE-SEM, respectively. The Fourier transform infrared (FTIR) and Raman spectroscopies were carried out to investigate the related agents on the surface of treated Al2024 powder and CNTs. The Raman intensity was recorded in four decimal places with a concentration measurement error of ±0.03 pct. Also, X-ray diffraction (XRD) analysis was performed to study the initial Al2024 powder and formed phases after the ball milling process.

III. RESULTS AND DISCUSSION

The main obstacle in production of homogenous dispersed Al2024–CNT nanocomposite powder is the geometrical differences between constituents, which results from the macro-metric scale and three-dimensional (3D) structure of the matrix in contrast with the nano-metric nature and one-dimensional (1D) characteristic of the reinforcement. The morphological changes of Al2024 powder to obtain a 2D flaky shape with a large diameter-to-thickness (D/t) aspect ratio can be considered to be a solution for the mentioned problem based on the FPM procedure. As a result, the D/t ratio of the Al2024 matrix is more in line with the length-to-diameter aspect ratio (L/D) of CNTs.

Figures 3, 4, 5, and 6 show SEM images related to the morphological changes of Al2024 powder after ball milling at different conditions. The ball milling process has been performed to achieve the uniform flaky shape

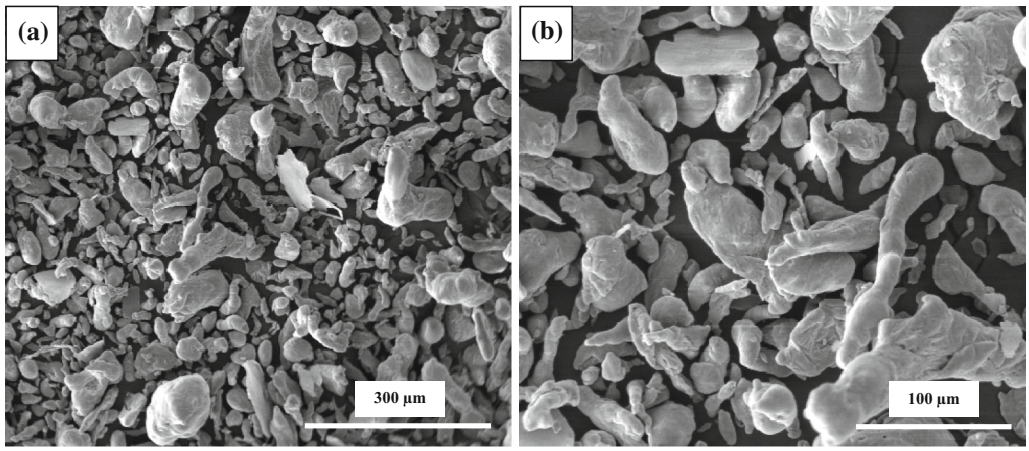

Fig. 3—SEM images of Al2024 powder after ball milling for 2 h, 250 rpm, BPR = 10 at two different magnifications.

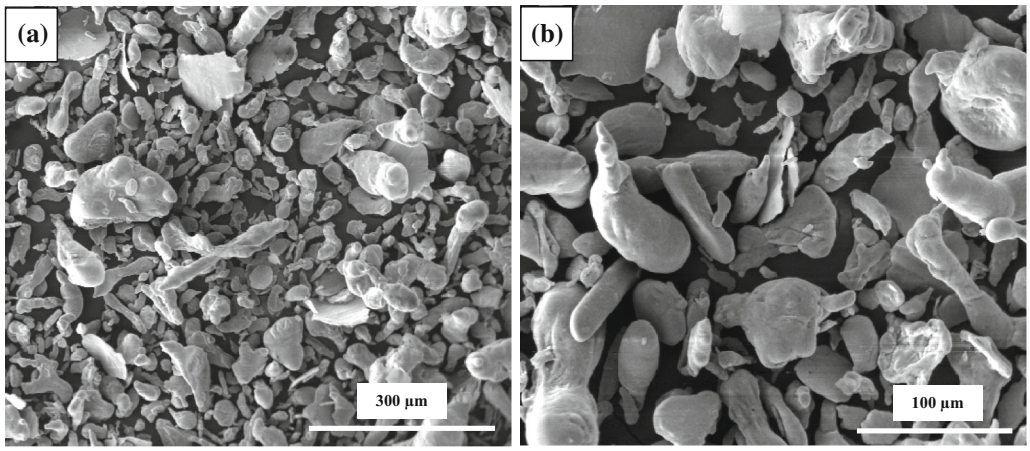

Fig. 4—SEM images of Al2024 powder after ball milling for 3 h, 250 rpm, BPR = 10 at two different magnifications.

of Al2024 powder. The effects of time and BPR as important variables have been studied in these figures. It should be considered that the parameter of time has the key role in obtaining a flake microstructure in matrix powder (step 1 of FPM).

As shown in Figure 3 at two different magnifications, the ball milling of Al2024 powder for 2 hours, rotation speed of 250 rpm, and BPR = 10 could lead to deformation of a small fraction of powder. In the other words, the energy of ball milling was not sufficient to reach the fully flake-shaped powder.

Figure 4 indicates that the amount of flaky powders has been raised in the microstructure by increasing the ball milling time to 3 hours, but the initial disordered morphology of Al2024 powder has still been observed in high regions. It seems that the morphological changes of Al2024 powder are needed to use a longer ball milling time or higher energy condition in comparison with pure Al powder, which has been reported in our previous work.[34] According to Figure 5, the complete flake-like morphology of Al2024 powder has resulted in ball milling at 250 rpm for 4 hours and BPR = 10. The geometrical properties of this uniform flaky shape Al2024 powder were involved in an average thickness of 1.53 μm and the mean diameter of 130 μm (D/t = 85). The microrolling deformation has been suggested as a simulative mechanism to elucidate the morphological changes of Al2024 powder.[31] The stainless steel balls can work as rollers in the ball milling process and the initial disordered powders are deformed between them to achieve the final laminated flakes. Consequently, the geometrical characteristics of the Al2024 matrix (D/t = 85) and CNT fibers (average L/D = 70) have become more comparable in this state, which can lead to an increase of chemical reactions probability between constituents during the mixing process (Figure 5(c)). Nevertheless, the nano-flake product with nanometer scale of thickness has not been obtained from Al2024 powder due to the large initial dimensions of disordered powder (Figure 5(d)).

Although the thickness value of 800 nm and D/t = 125 have resulted for flake-shaped pure Al powder with an initial average size less than 20 μm after the ball milling process for 2 hours at 200 rpm, which was formerly presented by the authors.[34]

Figure 6 shows SEM images of Al2024 powder with the same applied ball milling conditions in a previous state except the BPR parameter, which has been increased to 20. It is clearly observed that the higher energy level in planetary ball mill could also change the

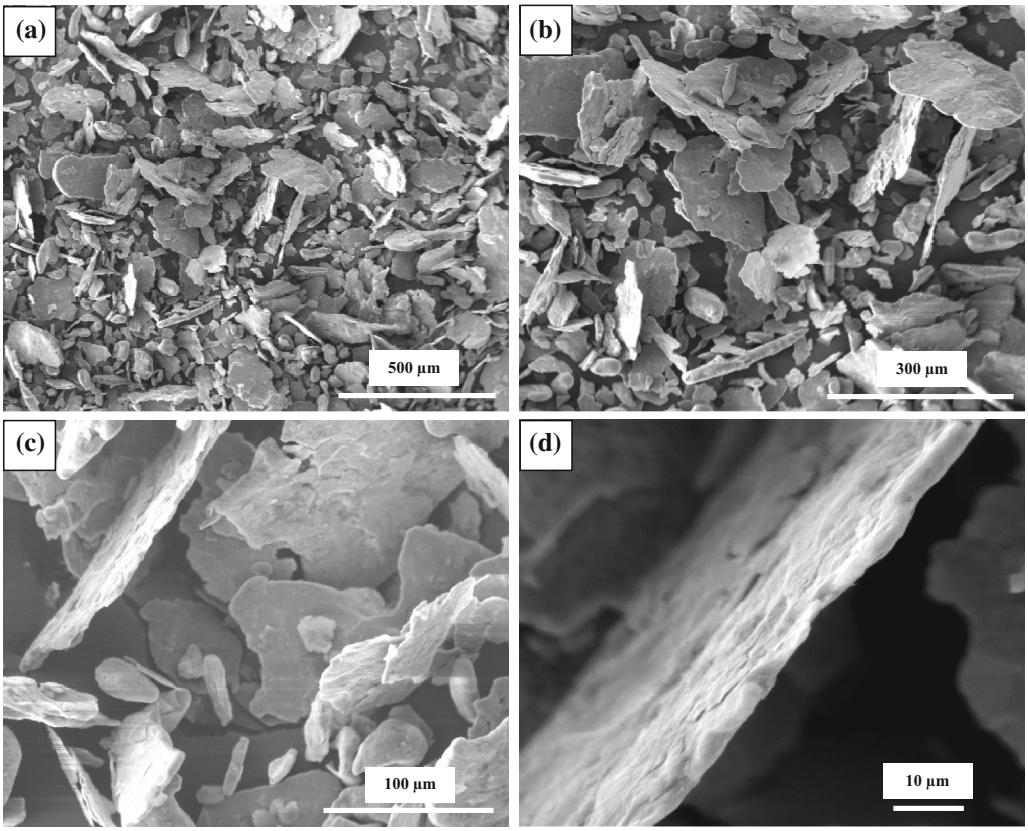

Fig. 5—SEM images of Al2024 powder after ball milling for 4 h, 250 rpm, BPR = 10 at four different magnifications.

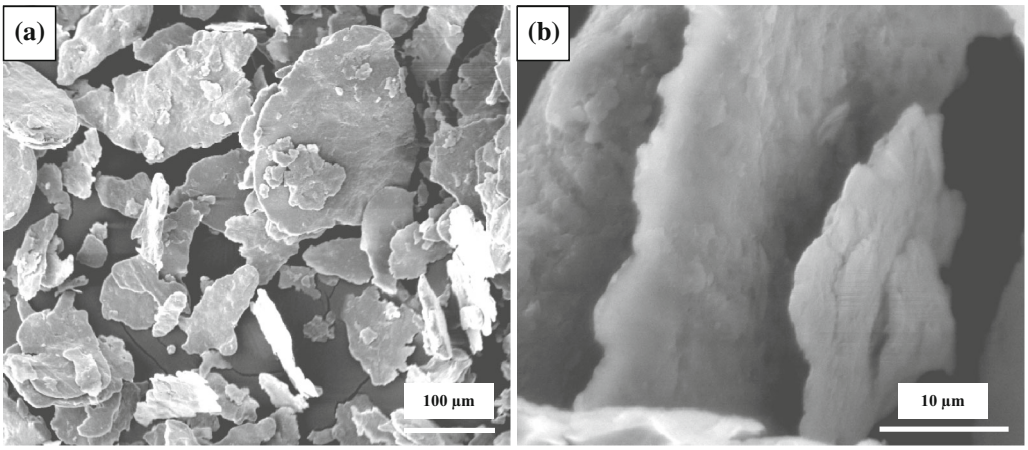

Fig. 6—SEM images of Al2024 powder after ball milling for 4 h, 250 rpm, BPR = 20 at two different magnifications.

morphology of Al2024 powder to the final flaky shape (Figure 6(a)). Although this figure demonstrates the formation of folded flake Al2024 powders that were stuck together (Figure 6(b)), it would be predictably continued to reach the final equiaxed microstructure.[35,36] It is important to know that the folded shape of matrix powder is not favorable in composite manufacturing due to the lower effective surface contact in reactions. Also, using a high-energy ball milling process can lead to work hardening of powders and it may result in more difficult absorption of CNTs in the mixing step. Additionally, it probably creates some problems in compaction of powders during the sintering or extrusion processes.

As a result, the product of ball milling process for 4 hours at 250 rpm and BPR = 10 was selected as a desired matrix in FPM processing of the Al2024–CNT nanocomposite.

The XRD patterns of Al2024 powder in two states of initial and after 4-hour ball milling are shown in Figure 7. According to this figure, all main peaks were related to Al in diffraction angles of 38, 45, 65, and 78

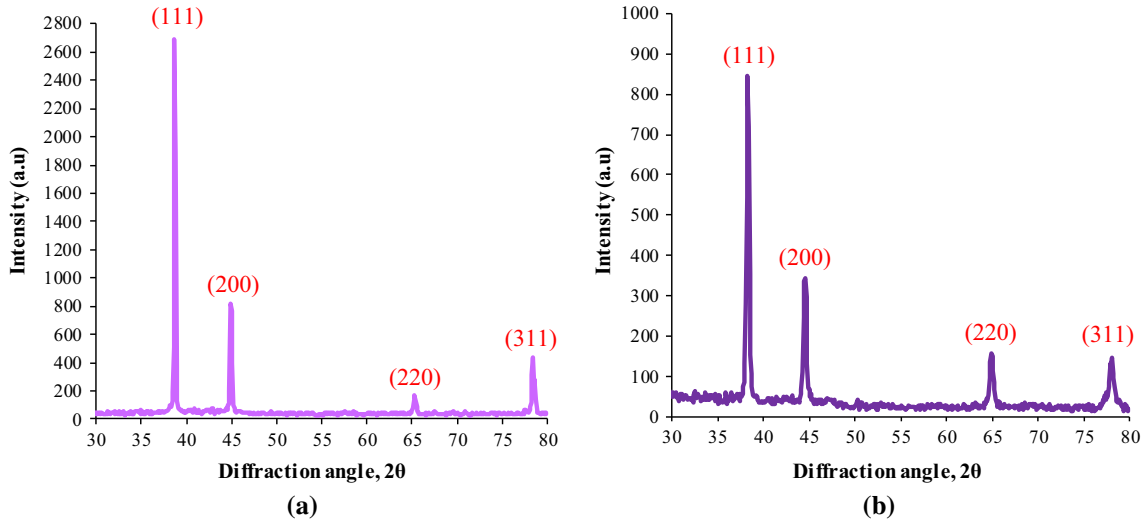

Fig. 7—XRD analysis curves of Al2024 powder: (*a*) initial and (*b*) after ball milling for 4 h.

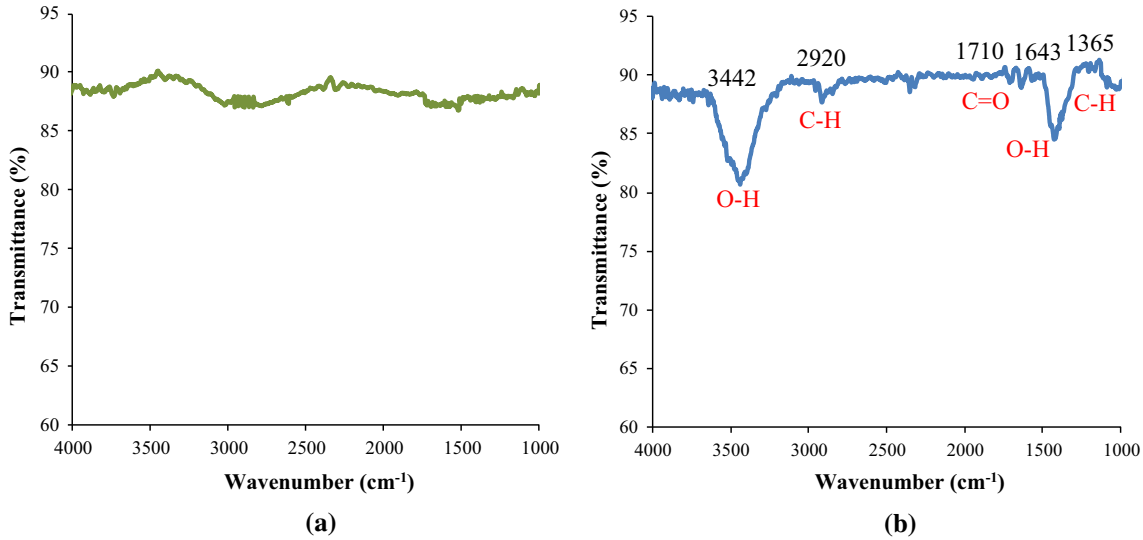

Fig. 8—FTIR patterns of carbon nanotubes: (*a*) before and (*b*) after refluxing by nitric acid.

deg in agreement with crystallographic planes of (111), (200), (220), and (311), respectively, for ball-milled Al2024 alloy, which is the same as the primary powder. In some other studies, the formation of intermetallic phases has been reported in a longer ball milling process.[37,38]

After morphological modification of Al2024 powders, the chemical improvement of Al2024 matrix and CNT reinforcement was performed by PVA coating and nitric acid refluxing, respectively. Figure 8 shows the FTIR results of CNTs before and after surface treatment. As shown in this figure (Figure 8(b)), the special bonds of C = O, C–H, and O–H, which were related to the carboxyl (–COOH) agent have been clearly formed after the refluxing process in the wavenumber of 1710, 2920, and 3442 cm^{-1}, respectively. But the initial CNTs have not shown any distinct peaks in this diagram (Figure 8(a)).

The effect of the refluxing process on the structure of CNTs was studied by Raman spectroscopy. As demonstrated in Figure 9, the I_D/I_G ratio, which was applied as a criterion for defect density and damage incurred to CNTs while processing, has not been considerably changed by refluxing in nitric acid. Moreover, the I_D/I_G ratio of 1.598 for CNT-COOH (Figure 9(b)) shows some decrease in comparison of initial state, which may be due to the elimination of impurities (step 2 of FPM).

The FTIR results for Al2024 powder in two states of uncoated and coated by PVA are demonstrated in Figure 10 (step 3 of FPM).

According to the curve of Al2024-PVA powder (Figure 10(b)), the bands at 3401 and 1342 cm^{-1} were allocated to the O–H stretch and bend vibrations, respectively. The other bands at 1070 and 1410 cm^{-1} corresponded to the O–H and C–H bend vibrations, which resulted from the PVA coating of Al2024 powder.

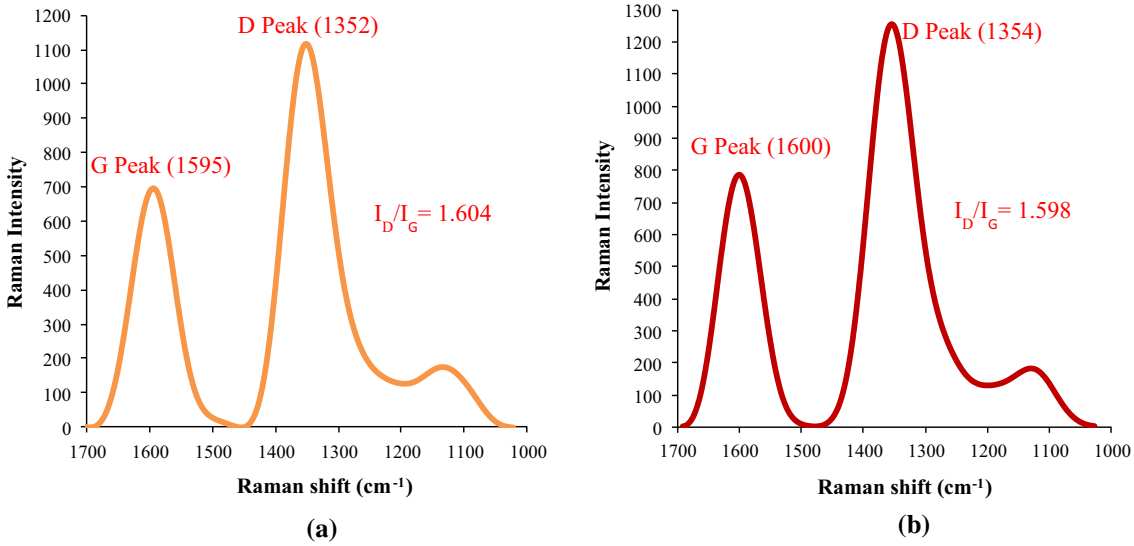

Fig. 9—Raman spectrum of carbon nanotubes: (*a*) before and (*b*) after refluxing by nitric acid.

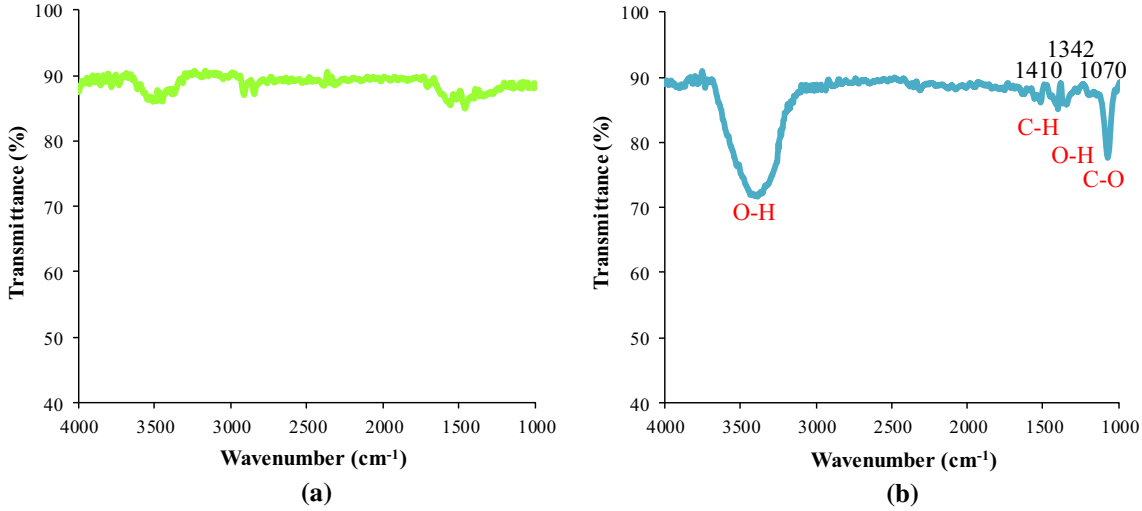

Fig. 10—FTIR patterns of Al2024 powder: (*a*) untreated and (*b*) coated with the PVA.

The uncoated Al2024 powder has not shown any significant band in the FTIR spectrum (Figure 10(a)), except in small peaks due to the existent humidity in powder. Consequently, the FTIR results confirmed the existence of PVA membrane on the Al2024 powder surface. It seems, then, that a suitable condition has been made to perform the chemical reaction between the –OH groups of PVA on Al2024 surface and –COOH agents of functionalized CNTs during the FPM process.

The final microstructure of the Al2024–CNT nanocomposite that resulted from the FPM procedure is shown in Figure 11 in different regions. It was perceived that the FPM method succeeded in producing the homogenous distribution of CNTs in the Al2024 matrix without any specific agglomeration of CNTs (Figures 11(a, b)). Also the soundness of CNT fibers has been saved during the FPM process (Figure 11(c)) and the complete absorption of CNTs could be observed on the surface of Al2024 powder (Figure 11(d)).

The dispersion mechanism of CNTs can be explained in physical and chemical issues. From physical point of view, the visual color changes and variation of pH criteria should be noticed. The suspension was finally stabilized at pH 5 when the Al2024–CNTs nanocomposite powder was settled in the bottom of the vessel, immediately after turning the magnetic stirrer off (step 4 of FPM). Lastly, the color of suspension was changed from initial ink-like to transparent (Figure 12).

The chemical predictable mechanism of CNTs dispersion within the Al2024 matrix is demonstrated in Figure 13. The main advantage of the FPM process was defined by the formation of hydrogen bonding between the superficial agents of constituents before drying of nanocomposite powder (Figure 13(c)). As a result, the CNTs were compelled to a chemical reaction with the Al2024 matrix in a fluid environment, and the opportunity of second congregation of CNTs due to the severe

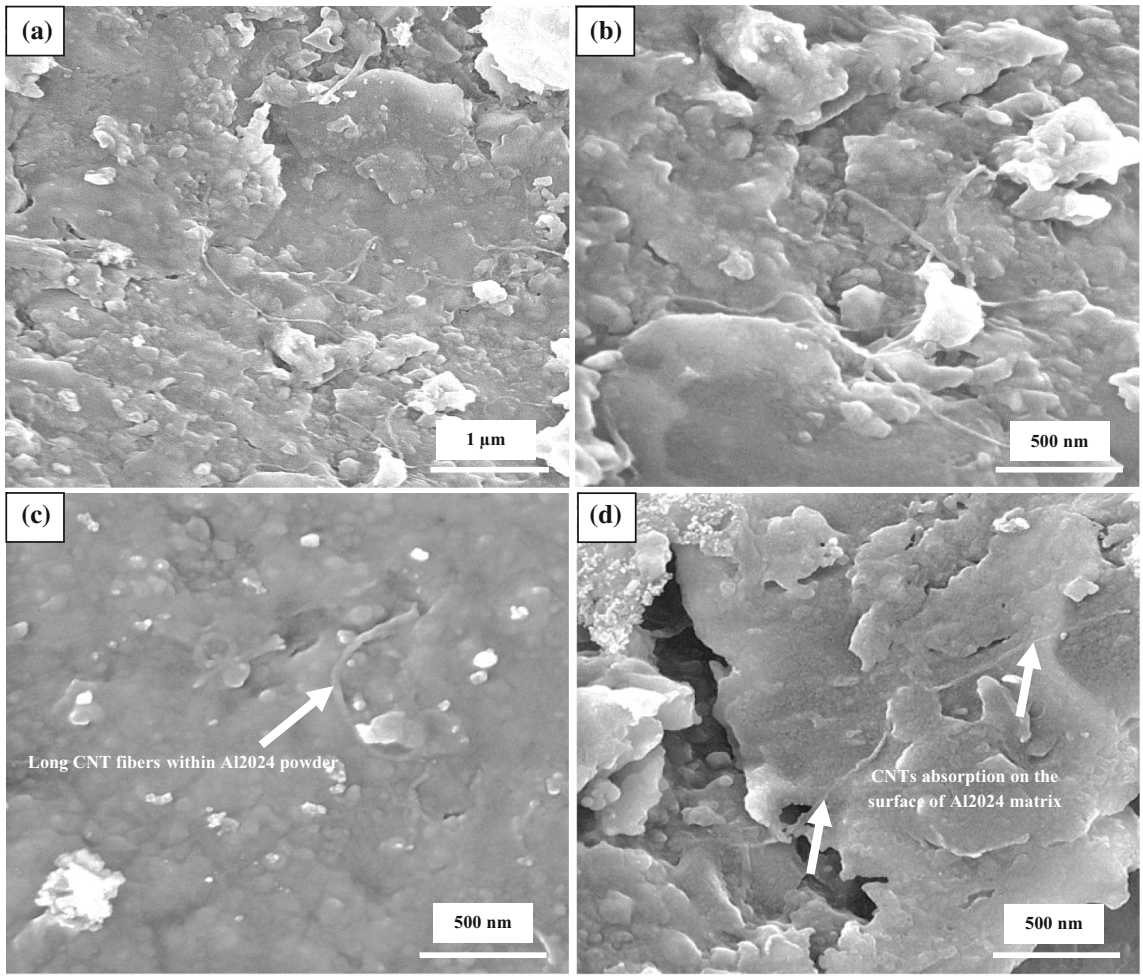

Fig. 11—Microstructure of Al2024–1.5 wt pct CNT composites in different regions.

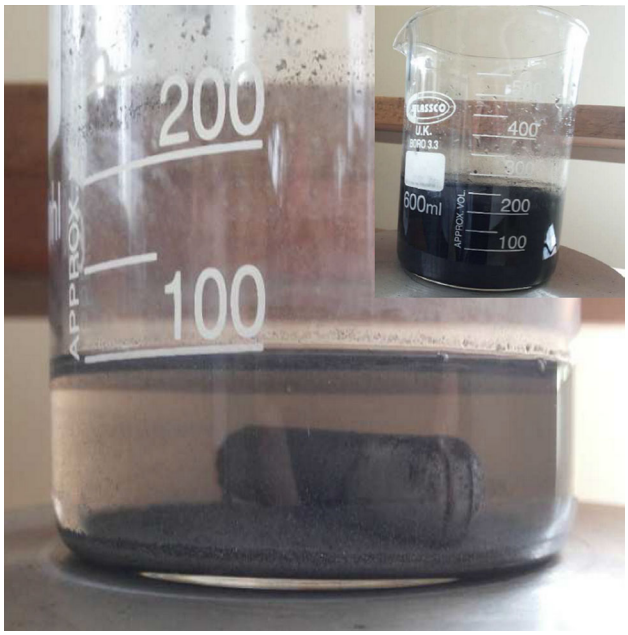

Fig. 12—Color change of Al–CNT suspension from dark to transparent at the end of mixing process.

van der Waals forces between them would be prevented before the drying step.

Also, by adding the diluted nitric acid in suspension of Al2024-PVA powder and decreasing pH to pH 3 before the mixing step, the hydrolysis of HNO_3 occurred and the ions of H^+ and NO_3^- were created in suspension. Therefore, the H^+ ions had the potential to attach the Al2024 surface with a thin layer of Al_2O_3 and a large amount of –OH groups due to the PVA overlay coating.

In other words, the SDS anionic surfactant in aqueous solution of CNTs could cause the formation of hydrophilic negative ions of $C_{12}H_{25}SO_4^-$ on the surface of CNTs. Consequently, a temporary polarity could be made during the mixing process between the H^+ and $C_{12}H_{25}SO_4^-$ ions on the surface of constituents, and this phenomenon assisted in complete absorption of CNTs on the Al2024 surface, besides the factor of the hydrogen bonding reaction.

IV. CONCLUSIONS

The main conclusions of this work can be drawn as follows:

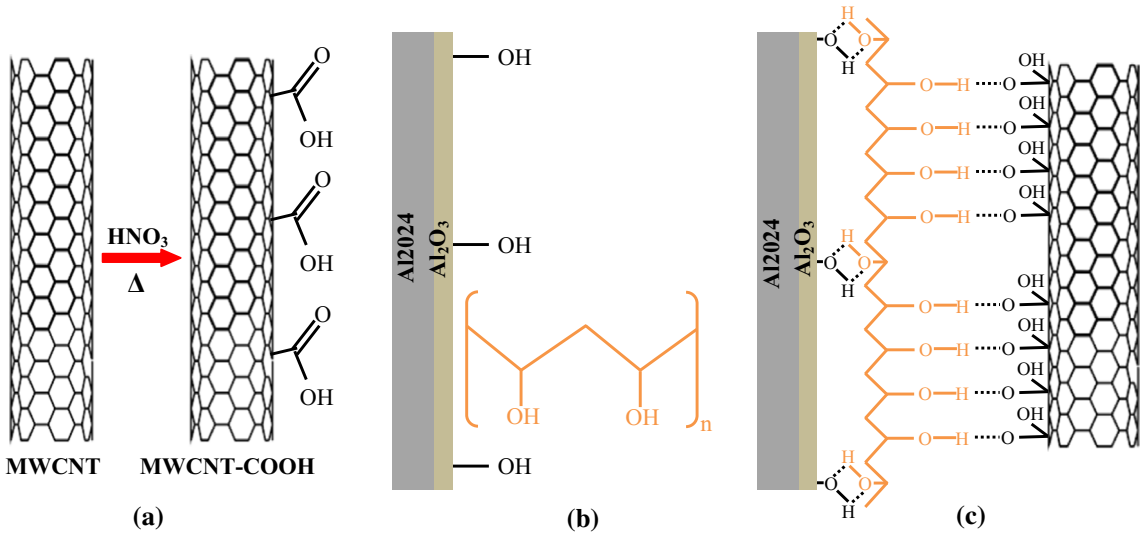

Fig. 13—Brief steps of flake powder metallurgy route: (*a*) functionalization of CNTs to obtain carboxyl agents on the surface by refluxing in nitric acid, (*b*) surface modification of Al2024 powder with PVA coating, and (*c*) formation of hydrogen bonding between –COOH groups of CNTs and –OH groups of Al2024-PVA powder.

(1) The FPM method, consisting of five main steps, produced the well-dispersed CNTs within Al2024 powder with chemical and structural modifications. The FPM process was quantified by controlling the ball milling variables to produce Al2024 flakes and pH of Al2024–CNT nanocomposite suspension to achieve steady state.

(2) The complete flake microstructure of Al2024 powder was obtained after ball milling for 4 hours at 250 rpm and BPR = 10 with an average thickness of 1.53 μm and the mean diameter of 130 μm (D/t = 85). XRD analysis showed only Al peaks after ball milling of Al2024 powder, which were the same as the initial one.

(3) The chemical modification of Al2024 powder and CNTs was performed by PVA coating and refluxing in nitric acid, respectively. The FTIR experiment confirmed the related bonds of –OH groups and –COOH agents on the surface of constituents after treatment of initial materials. The protection of CNTs during the refluxing step was verified by Raman spectroscopy.

(4) The suitable dispersion of CNT fibers within Al2024 flake-like powder resulted in the formation of hydrogen bonding between –OH groups of PVA-coated Al2024 and –COOH groups on CNT walls during the mixing step. Consequently, the homogeneity of CNT dispersion was obtained using the chemical reaction between the matrix and the reinforcement without applying any mechanical forces to unbundle CNTs.

(5) The CNTs distribution was affected by adding the diluted nitric acid to reach pH 3. It could cause the formation of temporary polarity between H^+ and $C_{12}H_{25}SO_4^-$ ions on the surface of constituents, and finally, the suspension was stabilized at pH 5 with changing of color from initial ink-like to the transparent.

ACKNOWLEDGMENTS

The authors are thankful to the Center of Excellence for High Strength Alloys Technology (CEHSAT) of IUST University. They also thank the support of the Iran National Science Foundation (INSF).

REFERENCES

1. A. Agarwal, S. Bakshi, and D. Lahiri: *Carbon Nanotubes: Reinforced Metal Matrix Composites*, 1st ed., Taylor and Francis, Boca Raton, 2011, pp. 1–70.
2. D. Phuong, P. Van Trinh, N. An, and N. Luan: *J. Alloys Compd.*, 2014, vol. 613, pp. 68–73.
3. X. Zeng, G. Zhou, Q. Xu, and Y. Xiong: *Mater. Sci. Eng. A*, 2010, vol. 527, pp. 5335–40.
4. J. Liao and M. Tan: *Powder Technol.*, 2011, vol. 208, pp. 42–48.
5. T. Laha, Y. Chen, D. Lahiri, and A. Agarwal: *Composites A*, 2009, vol. 40, pp. 589–94.
6. S. Salimi, H. Izadi, and A. Gerlich: *J. Mater. Sci.*, 2011, vol. 46, pp. 409–15.
7. H. Asgharzadeh, S. Joo, and H.S. Kim: *Metall. Mater. Trans. A*, 2014, vol. 54, pp. 4129–37.
8. J. Liao and M. Tan: *Mater. Lett.*, 2011, vol. 65, pp. 2742–44.
9. S. Yoo and W. Kim: *Mater. Sci. Eng. A*, 2013, vol. 570, pp. 102–05.
10. S. Yoo, S. Han, and W. Kim: *Scripta Mater.*, 2013, vol. 68, pp. 711–14.
11. Y. Wu and G. Kim: *J. Mater. Process. Technol.*, 2011, vol. 211, pp. 1341–47.
12. R. Pérez-Bustamante, F. Pérez-Bustamante, and I. Estrada-Guel: *Powder Technol.*, 2011, vol. 212, pp. 390–96.
13. Z. Liu, B. Xiao, W. Wang, and Z. Ma: *Carbon*, 2012, vol. 50, pp. 1843–52.
14. S. Simoes, F. Viana, M. Reis, and M. Vieira: *Compos. Struct.*, 2015, vol. 126, pp. 114–22.
15. D. Chunfeng, Z. Xuexi, and W. Dezun: *Mater. Lett.*, 2007, vol. 61, pp. 904–07.
16. D. Poirier, R. Gauvin, and R. Drew: *Composites A*, 2009, vol. 40, pp. 1482–89.
17. A. Esawi, K. Morsi, A. Sayed, and A. Gawad: *Mater. Sci. Eng. A*, 2009, vol. 508, pp. 167–73.
18. R. Perez-Bustamante, I. Estrada-Guel, P. Amezaga-Madrid, and M. Miki-Yoshida: *J. Alloys Compd.*, 2010, vol. 495, pp. 399–402.

19. R. Pérez-Bustamante, C. Gómez-Esparza, and I. Estrada-Guel: *Mater. Sci. Eng. A*, 2009, vol. 502, pp. 159–63.
20. A. Esawi, K. Morsi, A. Sayed, and M. Taher: *Compos. Sci. Technol.*, 2010, vol. 70, pp. 2237–41.
21. L. Wang, H. Choi, J. Myoung, and W. Lee: *Carbon*, 2009, vol. 47, pp. 3427–33.
22. R. Pérez-Bustamante, F. Pérez-Bustamante, I. Estrada-Guel, and L. Jiménez: *Mater. Charact.*, 2013, vol. 75, pp. 13–19.
23. B. Chen, S. Li, H. Imai, and L. Jia: *Mater. Des.*, 2015, vol. 72, pp. 1–8.
24. S. Simoes, F. Viana, M. Reis, and M. Vieira: *Compos. Struct.*, 2014, vol. 108, pp. 992–1000.
25. H. Choi, L. Wang, D. Cheon, and W. Lee: *Compos. Sci. Technol.*, 2013, vol. 74, pp. 91–98.
26. H. Kwon, M. Estili, K. Takagi, and T. Miyazaki: *Carbon*, 2009, vol. 47, pp. 570–77.
27. H. Kwon, D. Park, J. Silvain, and A. Kawasaki: *Compos. Sci. Technol.*, 2010, vol. 70, pp. 546–50.
28. H. Kwon, M. Takamichi, A. Kawasaki, and M. Leparoux: *Mater. Chem. Phys.*, 2013, vol. 138, pp. 787–93.
29. J. Tang, G. Fan, Z. Li, and X. Li: *Carbon*, 2013, vol. 55, pp. 202–08.
30. L. Jiang, Z. Li, G. Fan, and L. Cao: *Carbon*, 2012, vol. 50, pp. 1993–98.
31. L. Jiang, G. Fan, Z. Li, and X. Kai: *Carbon*, 2011, vol. 49, pp. 1965–71.
32. M. Jafari, M. Abbasi, M. Enayati, and F. Karimzadeh: *Adv. Powder Technol.*, 2012, vol. 23, pp. 205–10.
33. R. Pérez-Bustamante, M. González-Ibarra, and J. González-Cantú: *J. Alloys Compd.*, 2012, vol. 536, pp. 17–20.
34. F. Rikhtegar, S. Shabestari, and H. Saghafian: *Powder Technol.*, 2015, vol. 280, pp. 26–34.
35. J. Fuentes, J. Rodrigue, and E. Herrera: *Mater. Charact.*, 2010, vol. 61, pp. 386–95.
36. S. Khorasani, H. Abdizadeh, and S. Heshmati-Manesh: *Adv. Powder Technol.*, 2014, vol. 25, pp. 599–603.
37. R. Pérez-Bustamante, J. Escobedo, J. Lobato, and I. Estrada-Guel: *Wear*, 2012, vols. 292–3, pp. 169–75.
38. H. Choi, B. Min, J. Shin, and D. Bae: *Composites A*, 2011, vol. 42, pp. 1438–44.